1624 *Chem. Mater.* **2010,** *22,* 1624–1632
DOI:10.1021/cm9016276

CHEMISTRY OF MATERIALS
Article

# Mesoporous Ferromagnetic MPt@Silica/Carbon (M = Fe, Co, Ni) Composites As Advanced Bifunctional Catalysts

Emanuel Kockrick,[†] Franz Schmidt,[†] Kristina Gedrich,[†] Marcus Rose,[†] Thomas A. George,[‡] Thomas Freudenberg,[§] Ralph Kraehnert,[⊥] Ralph Skomski,[‡] David J. Sellmyer,[‡] and Stefan Kaskel*[,†]

[†]*Department of Inorganic Chemistry, Dresden University of Technology, Mommsenstrasse 6, D-01062 Dresden, Germany,* [‡]*Nebraska Center for Materials and Nanoscience−NCMN, University of Nebraska, Lincoln, Nebraska 68588,* [§]*Leibniz Institute for Solid State and Materials Research Dresden, Helmholtzstrasse 20, D-01069 Dresden, Germany, and* [⊥]*Department of Chemistry, Technical University of Berlin, Strasse des 17 Juni 124, D-10623 Berlin, Germany*

*Received June 18, 2009. Revised Manuscript Received October 27, 2009*

Ferromagnetic MPt (Fe, Co, Ni) nanocomposites were obtained by infiltration of aqueous and chloroform precursor solutions into ordered mesoporous SBA-15 and CMK-3. Channel-confined crystallization of the intermetallic phases was achieved under a reductive and inert atmosphere in a temperature range from 673 to 1073 K using conventional and ultrafast IR furnace heating. The proper choice of mesoporous matrix allows one to tailor crystallite size and to affect the phase transformation rate into ordered face-centered tetragonal (fct) MPt alloys. XRD and TEM techniques were used to monitor the structural evolution in the system. Physisorption methods reveal degradation of the mesoporous carbon matrix for MPt@CMK-3 composites while SBA-15 templated structures stay intact. SQUID investigations were carried out, demonstrating a strong dependence of magnetic properties on the intermetallic system, matrix, and treatment conditions. Especially for fct FePt@carbon, very high room-temperature coercivities up to 28.4 kOe were observed. The materials are efficient catalysts for acetylene to ethylene hydrogenation. Structure-sensitive selectivity of FePt is reported for the first time, demonstrating a higher selectivity of fct FePt composites as compared to the disordered face-centered cubic (fcc) phase.

## Introduction

Magnetic nanoparticle systems are potentially interesting materials in biotechnology and catalysis.[1−3] Especially, ordered platinum containing iron and cobalt alloys have received considerable attention during the past decade, because of their large uniaxial magnetocrystalline anisotropy constants causing ferromagnetic properties down to 2−3 nm appropriate for ultra high density storage devices.[4−10] Furthermore, these alloys show high saturation magnetizations and the high chemical stability needed in biomagnetic hyperthermia therapy.[11,12] In combination with appropriate matrices, magnetic intermetallic nanoparticles are also suitable as advanced bifunctional catalyst systems because of the facile separation and lower costs compared to pure noble metal systems.[13−15] In particular, the ordered alloys are attractive as selective catalysts because of their high coercivity.[16,17] These applications require a defined particle size and phase purity. However, during the synthesis in solution, the metastable disordered face-centered cubic (fcc) phase is formed and temperatures up to 873 K are necessary for the transformation into the desired face centered tetragonal (fct) modification.[6] The latter causes particle aggregation and grain growth lowering monodispersity and increasing particle size. Various physical and chemical synthesis strategies were developed for

*Corresponding author. E-mail: stefan.kaskel@chemie.tu-dresden.de. Phone: 49-351-46333632. Fax: 49-351-46337287.

(1) Lu, A. H.; Salabas, E. L.; Schueth, F. *Angew. Chem., Int. Ed.* **2007**, *46*, 1222.
(2) Hyeon, T. *Chem. Commun.* **2003**, 927.
(3) LesliePelecky, D. L.; Rieke, R. D. *Chem. Mater.* **1996**, *8*, 1770.
(4) Sellmyer, D. J. *Nature* **2002**, *420*, 374.
(5) Weller, D.; Moser, A. *IEEE Trans. Magn.* **1999**, *35*, 4423.
(6) Sun, S. H.; Murray, C. B.; Weller, D.; Folks, L.; Moser, A. *Science* **2000**, *287*, 1989.
(7) Sun, S. H.; Fullerton, E. E.; Weller, D.; Murray, C. B. *IEEE Trans. Magn.* **2001**, *37*, 1239.
(8) Zeng, H.; Li, J.; Liu, J. P.; Wang, Z. L.; Sun, S. H. *Nature* **2002**, *420*, 395.
(9) Yamamoto, S.; Morimoto, Y.; Tamada, Y.; Takahashi, Y. K.; Hono, K.; Ono, T.; Takano, M. *Chem. Mater.* **2006**, *18*, 5385.
(10) Chen, M.; Nikles, D. E. *J. Appl. Phys.* **2002**, *91*, 8477.
(11) Gu, H.; W.; Xu, K. M.; Xu, C. J.; Xu, B. *Chem. Commun.* **2006**, 941.
(12) Sun, S. H. *Adv. Mater.* **2006**, *18*, 393.
(13) Lu, A. H.; Li, W. C.; Kiefer, A.; Schmidt, W.; Bill, E.; Fink, G.; Schueth, F. *J. Am. Chem. Soc.* **2004**, *126*, 8616.
(14) Lu, A. H.; Schmidt, W.; Matoussevitch, N.; Boennemann, H.; Spliethoff, B.; Tesche, B.; Bill, E.; Kiefer, W.; Schueth, F. *Angew. Chem., Int. Ed.* **2004**, *43*, 4303.
(15) Son, S. U.; Jang, Y.; Park, J.; Na, H. B.; Park, H. M.; Yun, H. J.; Lee, J.; Hyeon, T. *J. Am. Chem. Soc.* **2004**, *126*, 5026.
(16) Sort, J.; Surinach, S.; Baro, M. D.; Muraviev, D.; Dzhardimalieva, G. I.; Golubeva, N. D.; Pomogailo, S. I.; Pomogailo, A. D.; Macedo, W. A. A.; Weller, D.; Skumryev, V.; Nogues, J. *Adv. Mater.* **2006**, *18*, 466.
(17) Jun, Y. W.; Choi, J. S.; Cheon, J. *Chem. Commun.* **2007**, 1203.
(18) Luo, C. P.; Liou, S. H.; Gao, L.; Liu, Y.; Sellmyer, D. J. *Appl. Phys. Lett.* **2000**, *77*, 2225.


Published on Web 02/11/2010

ordered homogeneous fct alloys.[12,18−20] Especially, the polyol method was widely studied for FePt. By varying the precursor systems, surfactant ratios, and treatment conditions, researchers could precisely control the resulting nanoparticle geometry, size, and phase structure.[8,21−23] Additionally, hard templated, inorganic matrix-assisted methods inside mesoporous silica,[24,25] alumina,[26] and titania[16] were developed.

In the following, we present the synthesis and characterization of intermetallic nanoparticles in the system MPt (M = Fe, Co, Ni) inside various ordered mesoporous materials. Especially, synthesis strategies for hexagonal ordered SBA-15 materials are extensively investigated.[27−29] The resulting materials are characterized by a defined pore structure, chemical resistance and high thermal stability.[30,31] Thus, ordered mesoporous materials are interesting as catalyst host systems.[32] Different nanoscale metal,[13,33] metal oxides,[34,35] and alloys[24,36] could be synthesized inside the pore system by in or ex situ methods.[37,38] Catalytic activity of the composites was demonstrated in hydrogenation,[39] olefin epoxidation,[40] and CO oxidation reactions.[41] In recent experiments, ordered mesoporous carbon CMK-3 templates obtained by silica nanocasting were also used for the preparation of catalyst systems.[42−44] In comparison to porous silica structures, carbon templates offer significantly higher

**Scheme 1. Synthesis Strategy for the Preparation of MPt Particles by Infiltration of Aqueous and Chloroform Precursor Solutions into the Pores of Ordered Mesoporous Silica SBA-15 (Upper Path) and Carbon CMK-3 (Lower Path) Followed by Thermal Treatment by a Two- (Indirect Treatment) and One-Step (Direct Treatment) Method to 673−1073 K in Regular and IR Furnace under Reductive and Inert Atmosphere**

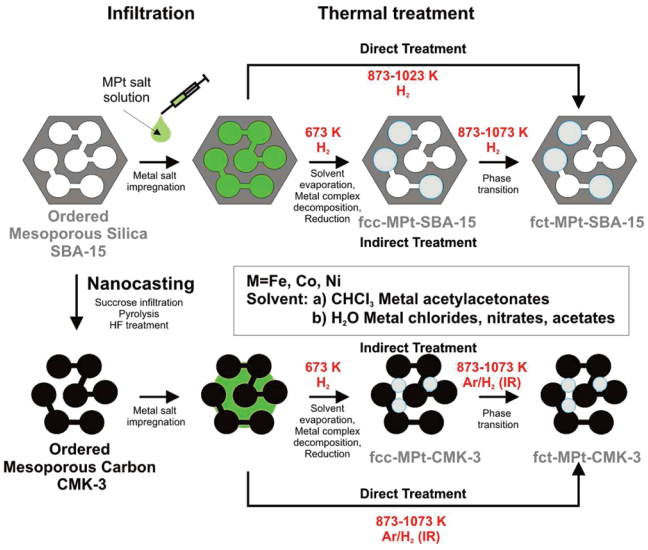


specific surface areas and biocompatibility.[14,45] Therefore, these materials are more suitable for biomagnetic applications. Various transition metal and oxide composite structures were already prepared using hexagonal ordered CMK-3 and CMK-5 templates.[46−49] In particular, templated bimetallic nanoparticle systems are potentially interesting for comprehensive catalytic applications because of their composition and resulting electronic structure.[17] Different groups have already demonstrated the catalytic activity of alloy nanostructures on porous carbon templates in selective hydrogenation reactions[50] and in electrocatalysis like direct methanol fuel cell applications.[51,52] However, so far there are only a few reports in the literature for the catalytic application of ferromagnetic nanoscale alloys templated inside ordered mesoporous materials.[39]

The schematic synthesis strategy for the preparation of magnetic nanoparticles is shown in Scheme 1. Our efforts are focused on the synthesis of ordered platinum containing alloys (MPt; M = Fe, Co, Ni). In the first step, hexagonal ordered mesoporous silica SBA-15 and the carbon replica structure CMK-3 were infiltrated with aqueous and chloroform solutions of soluble M and Pt precursor metal compounds, respectively. To remove the organic compounds and initialize the reduction process,

(19) Luo, C. P.; Liou, S. H.; Sellmyer, D. J. *J. Appl. Phys.* **2000**, *87*, 6941.
(20) Elkins, K. E.; Vedantam, T. S.; Liu, J. P.; Zeng, H.; Sun, S. H.; Ding, Y.; Wang, Z. L. *Nano Lett.* **2003**, *3*, 1647.
(21) Zeng, H.; Li, J.; Wang, Z. L.; Liu, J. P.; Sun, S. H. *Nano Lett.* **2004**, *4*, 187.
(22) Wang, Y.; Yang, H. *J. Am. Chem. Soc.* **2005**, *127*, 5316.
(23) Wang, C.; Hou, Y. L.; Kim, J. M.; Sun, S. H. *Angew. Chem., Int. Ed.* **2007**, *46*, 6333.
(24) King, N. C.; Blackley, R. A.; Wears, M. L.; Newman, D. M.; Zhou, W. Z.; Bruce, D. W. *Chem. Commun.* **2006**, 3414.
(25) Kockrick, E.; Krawiec, P.; Schnelle, W.; Geiger, D.; Schappacher, F. M.; Pottgen, R.; Kaskel, S. *Adv. Mater.* **2007**, *19*, 3021.
(26) Bian, B.; Laughlin, D. E.; Sato, K.; Hirotsu, Y. *J. Appl. Phys.* **2000**, *87*, 6962.
(27) Beck, J. S.; Vartuli, J. C.; Roth, W. J.; Leonowicz, M. E.; Kresge, C. T.; Schmitt, K. D.; Chu, C. T. W.; Olson, D. H.; Sheppard, E. W.; McCullen, S. B.; Higgins, J. B.; Schlenker, J. L. *J. Am. Chem. Soc.* **1992**, *114*, 10834.
(28) Corma, A. *Chem. Rev.* **1997**, *97*, 2373.
(29) Zhao, D. Y.; Feng, J. L.; Huo, Q. S.; Melosh, N.; Fredrickson, G. H.; Chmelka, B. F.; Stucky, G. D. *Science* **1998**, *279*, 548.
(30) Ying, J. Y.; Mehnert, C. P.; Wong, M. S. *Angew. Chem., Int. Ed.* **1999**, *38*, 56.
(31) Davis, M. E. *Nature* **2002**, *417*, 813.
(32) Taguchi, A.; Schueth, F. *Microporous Mesoporous Mater.* **2005**, *77*, 1.
(33) Han, Y. J.; Kim, J. M.; Stucky, G. D. *Chem. Mater.* **2000**, *12*, 2068.
(34) Froeba, M.; Kohn, R.; Bouffaud, G.; Richard, O.; van Tendeloo, G. *Chem. Mater.* **1999**, *11*, 2858.
(35) Kohn, R.; Froeba, M. *Catal. Today* **2001**, *68*, 227.
(36) Mizutani, M.; Yamada, Y.; Nakamura, T.; Yano, K. *Chem. Mater.* **2008**, *20*, 4777.
(37) Krawiec, P.; Kockrick, E.; Simon, P.; Auffermann, G.; Kaskel, S. *Chem. Mater.* **2006**, *18*, 2663.
(38) Wang, Q.; Shantz, D. F. *J. Solid State Chem.* **2008**, *181*, 1659.
(39) Gupta, G.; Patel, M. N.; Ferrer, D.; Heitsch, A. T.; Korgel, B. A.; Jose-Yacaman, M.; Johnston, K. P. *Chem. Mater.* **2008**, *20*, 5005.
(40) Shokouhimehr, M.; Piao, Y. Z.; Kim, J.; Jang, Y. J.; Hyeon, T. *Angew. Chem., Int. Ed.* **2007**, *46*, 7039.
(41) Wang, A.; Q.; Chang, C. M.; Mou, C. Y. *J. Phys. Chem. B* **2005**, *109*, 18860.
(42) Ryoo, R.; Joo, S. H.; Jun, S. *J. Phys. Chem. B* **1999**, *103*, 7743.
(43) Ryoo, R.; Joo, S. H.; Kruk, M.; Jaroniec, M. *Adv. Mater.* **2001**, *13*, 677.
(44) Lu, A.; Schueth, F. *Adv. Mater.* **2006**, *18*, 1793.
(45) Bazula, P. A.; Lu, A. H.; Nitz, J. J.; Schueth, F. *Microporous Mesoporous Mater.* **2008**, *108*, 266.
(46) Joo, S. H.; Pak, C.; You, D. J.; Lee, S. A.; Lee, H. I.; Kim, J. M.; Chang, H.; Seung, D. *Electrochim. Acta* **2006**, *52*, 1618.
(47) Huwe, H.; Froeba, M. *Microporous Mesoporous Mater.* **2003**, *60*, 151.
(48) Schwickardi, M.; Olejnik, S.; Salabas, E. L.; Schmidt, W.; Schueth, F. *Chem. Commun.* **2006**, 3987.
(49) Park, I. S.; Choi, M.; Kim, T. W.; Ryoo, R. *J. Mater. Chem.* **2006**, *16*, 3409.
(50) Vu, H.; Goncalves, F.; Philippe, R.; Lamouroux, E.; Corrias, M.; Kihn, Y.; Plee, D.; Kalck, P.; Serp, P. *J. Catal.* **2006**, *240*, 18.
(51) Chai, G. S.; Yoon, S. B.; Yu, J. S.; Choi, J. H.; Sung, Y. E. *J. Phys. Chem. B* **2004**, *108*, 7074.
(52) Welch, C. W.; Compton, R. G. *Anal. Bioanal. Chem.* **2006**, *384*, 601.

**Table 1. Sample Composition for the Preparation of MPt Silica and Carbon Composites by Infiltration of Aqueous and Chloroform Precursor Salt Solutions**

| | aqueous solution | | | chloroform solution | | |
|---|---|---|---|---|---|---|
| system | Fe/Pt | Co/Pt | Ni/Pt | Fe/Pt | Co/Pt | Ni/Pt |
| $n/1 \times 10^{-4}$ (mol) | 1.6 /1.6 | | | 1.6/1.6 | | 0.8/0.8 |
| $m_{meso}$ (g) | 0.2 | | | 0.2 | | |
| $V_{SBA-15}$ (mL) | 0.26 | | | 0.4 | | |
| $V_{CMK-3}$ (mL) | 0.18 | | | 0.4 | | |

we heat-treated compounds in a two-step mechanism first to 673 K and then 1023 K (indirect treatment).[25] For comprehensive investigations, composites are annealed in an infrared (IR) furnace, reducing the annealing time to minimize particle aggregation. Additionally, a direct treatment pathway is applied heating the carbon and the silica composites directly to 873−1073 K in IR or regular furnace, respectively.

## Experimental Section

All chemicals were used as received.

**Synthesis of SBA−15.** [60] Pluronic (8.1 g, $EO_{20}PO_{70}EO_{20}$ P123, Aldrich) was dissolved in 146.8 g of deionized water and 4.4 g of conc. HCl (37%) and stirred overnight at 308 K in a closed 250 mL one-neck flask. To this solution was quickly added 16 g of TEOS (Aldrich 98%) and the solution was stirred for 20 h at 308 K. The milky suspension was transferred to an autoclave and annealed at 403 K for 24 h. The solid product was filtered, washed with an HCl/water mixture, and calcined at 823 K.

**Synthesis of CMK-3.** [61] Ordered mesoporous carbon CMK-3 was synthesized according to a method reported by Jun et al. by double infiltration and drying technique of acid aqueous sucrose solution as carbon source into SBA-15 host followed by pyrolysis and silica removal using NaOH solution.

**Synthesis of MPt/CMK-3, SBA-15 Composites.** Equimolar ratios of $FeCl_2 \cdot 4H_2O$ (ABCR, 99%), $CoCl_2 \cdot 6H_2O$ (ABCR, 98%), $Ni(CH_3COO)_2 \cdot 6H_2O$ (Sigma Aldrich, 98%) and $H_2PtCl_6 \cdot 6H_2O$ (ABCR, 98%, 40 wt % Pt) were employed as aqueous precursors and are presented in Table 1. The water content of hexachloro platinic acid was estimated by DSC/TG measurements up to a molar ratio of 6.12. For the preparation of the aqueous solution derived MPt composites, precursors were dissolved in 0.26 mL (SBA-15) and 0.18 mL (CMK-3) of deionized water, respectively, and infiltrated by incipient wetness technique into activated ordered mesoporous silica and carbon. The solvent amount was calculated according to the specific pore volume estimated by nitrogen physisorption measurements at $p/p_0 = 0.975$ of pristine SBA-15 and CMK-3 starting materials. In comparison, equimolar amounts of $Fe(acac)_3$ (Sigma Aldrich, 99%), $Co(acac)_3$ (ABCR, 98%), $Ni(acac)_2$ (ABCR, 98%), and $Pt(acac)_2$ (ABCR, 98%) were dissolved in 0.4 mL of $CHCl_3$ (p.a. Fisher Scientific) and infiltrated into 0.2 g of the mesoporous host. The lower concentration of $Ni(acac)_2$ and $Pt(acac)_2$ solution is determined by the solubility of $Ni(acac)_2$ in $CHCl_3$. To decompose the metal salt and initialize the reduction process, we heat-treated carbon and silica composites in hydrogen flow from room temperature to 673 K (5 K/h) for 1 h in a regular furnace. In a second step, preannealed MPt composites were heat treated at 1023 K for 1 h in a regular furnace and at 1073 K for 20 min with an ultrafast heating ramp of 3 K/s in an infrared furnace (Behr IRF 10) in a reductive and inert atmosphere (Ar). For comprehensive investigations, precursor salt containing carbon and silica composites were annealed directly to 1073 K in IR and 1023 K standard furnace, respectively.

For the preparation of the 1 wt % FePt@SBA-15 composite for catalytic hydrogenation reactions, $4.03 \times 10^{-5}$ mol of $FeCl_2 \cdot 4H_2O$ and $4.03 \times 10^{-5}$ mol of $H_2PtCl_6 \cdot 6.12H_2O$ were dissolved in 1.3 mL of deionized water, infiltrated into 1 g of SBA-15 and heat treated first up to 673 K (sample code: **49**) and then to 1023 K (sample code: **50**).

**Catalytic Hydrogenation Reaction.** To elucidate activity, selectivity, and stability of FePt@SBA-15, with respect to the present FePt phase, we tested materials containing 1 wt % FePt as catalysts in the gas-phase hydrogenation of an acetylene/ethylene mixture. The tested materials are FePt@SBA-15 with present intermetallic fct phase treated at 1023 K as well as disordered fcc phase annealed at 673 K.

The hydrogenation was carried out in a continuous fixed-bed reactor setup operated in repeated temperature cycles between 313 and 373 K. For the test, 20 mg of catalyst were diluted 1:10 with SiC.[62] A gas mixture containing acetylene (1.7%), excess ethylene (42.9%), hydrogen (condition A, 3.4%; condition B, 2.1%), and nitrogen (balance) was continuously dosed to the reactor operated at 2 bar with a flow rate of 13.7 mL/min (STP). The temperature was increased from 313 to 373 K in 10 K steps, holding the temperature constant for about 3.3 h at each temperature, and repeating this program alternating with higher and lower hydrogen feed (i.e., conditions A, B).

**Characterization.** Wide-angle X-ray powder diffraction patterns were recorded in transmission geometry using a Stoe Stadi-P diffractometer and Cu $K\alpha_1$ radiation ($\lambda = 0.15405$ nm). Size broadening of reflections in the range $2\theta = 20-90°$ was analyzed using the Stoe size/strain analysis. Instrumental broadening was taken into account based on $LaB_6$ reference measurements. Samples for TEM analysis were prepared by dipping carbon coated copper grids into an ethanol suspension of MPt silica and carbon composites. TEM investigations were performed on a 200 kV-TEM FEI Tecnai T20 instrument. The small-angle X-ray experiments were carried out in transmission mode on a Bruker Nanostar with Cu $K\alpha_1$ radiation ($\lambda = 0.15405$ nm) and a position sensitive HiStar detector. Nitrogen physisorption isotherms were measured at 77 K using a Quantachrome Autosorb 1C apparatus. Prior to the measurement, the samples were activated in vacuum at 423 K for 24 h. Specific surface areas were calculated using the BET equation ($p/p_0 = 0.05-0.2$). The pore size distribution for carbon and silica composites was estimated from the adsorption branch using BJH theory. Water vapor physisorption measurements were carried out with Hydrosorb 1000 from Quantachrome at a temperature of 298 K. The pore volume for water vapor and nitrogen physisorption were determined at relative pressure $p/p_0 = 0.975$. The magnetization was measured in a SQUID magnetometer (MPMS XL-7, Quantum Design) from 2 to 298 K. The isothermal magnetization was measured with a solenoid in the hysteresis mode swept to ±5 and ±70 kOe.

## Results and Discussion

MPt composites were prepared by a single infiltration of stoichiometric amounts of the appropriate metal salts (MPt) dissolved in either chloroform or an aqueous solvent into ordered mesoporous SBA-15 or CMK-3 (Scheme 1). In order to form the ordered intermetallic alloys, the composites were heat treated in one of the two

**Table 2. Sample Codes, Crystallite Sizes, and Phase Structure of Intermetallic MPt Nanoparticles Inside Mesoporous Carbon and Silica Templates**

| | | sample code $d$ (nm)[a]/intermetallic phase[b] | | | | | | | | | | | |
|---|---|---|---|---|---|---|---|---|---|---|---|---|---|
| | | FePt | | | | CoPt | | | | NiPt | | | |
| | | indirect | | | direct | indirect | | | direct | indirect | | | direct |
| | | 673 | 1073 IR $H_2$/Ar | 1023 | 1073 IR /1073 | 673 | 1073 IR | 1023 | 1073 IR /1073 | 673 | 873 IR | 873 | 873 IR /873 |
| CMK −3 | $H_2O$ | **1** | **2** | **3** | **4** | **5** | **6** | **7** | **8** | **9** | **10** | **11** | **12** |
| | | 2.8 | 20.3 | 19.8 | 29.9 | 4.3 | 23.8 | 36.9 | 46.9 | 10.0 | 17.0 | 15.0 | 21.8 |
| | | fcc | fct | fct | fct | fcc | fcc(t) | fcc(t) | fcc(t) | fcc | mix | mix | fct |
| | $CHCl_3$ | **13** | **14** | **15** | **16** | **17** | **18** | **19** | **20** | **21** | **22** | **23** | **24** |
| | | < 2 | 7.8/2 | 9.6 | 7.3 | < 2 | 8.0 | 11.0 | 5.4 | < 2 | < 2 | < 2 | < 2 |
| | | | fct | fct | fct | | fct | fct | fcc(t) | | | | |
| SBA −15 | $H_2O$ | **25** | **26** | **27** | **28** | **29** | **30** | **31** | **32** | **33** | **34** | **35** | **36** |
| | | 6.2 | 8.3 | 10.6 | 7.5 | 9.0 | 29.8 | 16.2 | 10.6 | 8.7 | 8.2 | 9.9 | 10.4 |
| | | fcc | fcc(t) | fct | fct | fcc | $CoPt_3$ | $CoPt_3$ | fct | fcc/Ni | fcc/Ni | fcc/Ni | fcc/Ni |
| | $CHCl_3$ | **37** | **38** | **39** | **40** | **41** | **42** | **43** | **44** | **45** | **46** | **47** | **48** |
| | | < 2 | < 2 | < 2 | < 2 | < 2 | < 2 | < 2 | < 2 | < 2 | < 2 | < 2 | < 2 |

[a] Estimated by the (111) peak broadening of using Scherrer equation. [b] fcc, face-centered cubic (disordered alloy); fct, face-centered tetragonal (ordered intermetallic compound); mix, multiple nickel and platinum phases.

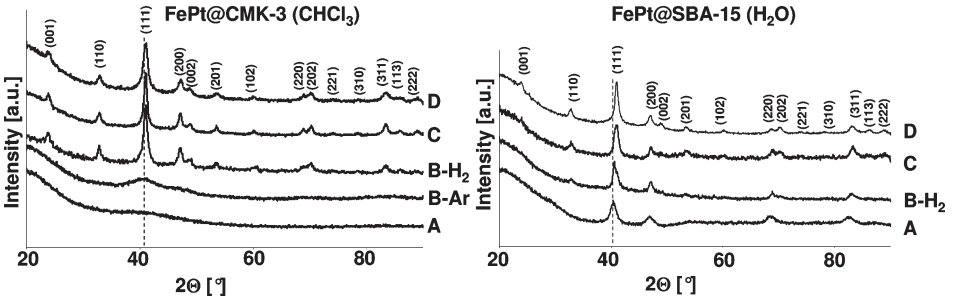


**Figure 1.** X-ray powder diffraction patterns of FePt@CMK-3 (**13**−**16**) and FePt@SBA-15 composites (**25**−**28**) synthesized by (A−C) indirect treatment at (A) 673 K, (B−Ar/$H_2$) 1073 K in IR furnace in argon and hydrogen atmosphere, and (C) 1023 K, and by direct pathway at (D) 1073 K using IR technique for FePt@CMK-3 and (D) 1023 K for FePt@SBA-15 composites, respectively.

illustrated pathways. One path, the indirect treatment, included heating first to 673 K and then up to 873−1073 K, similar to previous investigations.[25] To make a comprehensive study, some of the metal-salt containing matrices were annealed immediately to 873−1073 K (Scheme 1, direct treatment) using a conventional furnace and an IR furnace for ultra fast treatment. NiPt was treated only up to 873 K, because of the lower temperature of the face-centered tetragonal (fct) to face-centered cubic (fcc) phase transition as compared to bulk FePt and CoPt.[53−55]

**Structural Evolution of MPt: Wide-Angle X-ray Powder Diffraction/TEM Measurements.** The dependence of crystallinity and phase transformation of MPt compounds on synthesis conditions as investigated by wide-angle XRD is presented in Table 2, Figure 1, and the Supporting Information 1−5. According to the diffraction patterns, the MPt structure and crystallite size depend strongly on the infiltration route, the chemical and physical properties of the host matrix, the MPt system, and the thermal treatment conditions. As can be seen, the resulting crystallite sizes for MPt particles prepared by infiltration of aqueous solutions are significantly larger than chloroform solution derived systems. Similarly, the consequence of the different pore structures of the mesoporous host is demonstrated by its effect on the resulting crystallite sizes. In the highly interconnected CMK-3 structure, particles up to 47 nm (**8**) in diameter are found, whereas in the more isolated pores of silica, the diameter is much smaller.

Furthermore, the hydrophobicity of the matrix, as related to the polarity of the solvent, affects the degree of wetting and pore filling and therefore the particle size. Results of water vapor adsorption measurements carried out on the unloaded pore structures are presented in Supporting Information 6. The specific pore volume of mesoporous carbon estimated by water vapor measurements is 81% of the pore volume calculated from nitrogen physisorption measurements, indicating a more hydrophobic surface. In comparison, specific pore volumes of silanol group containing SBA-15 show a higher degree of hydrophilicity. They show similar values of 1.21 $cm^3/g$ for water vapor and 1.30 $cm^3/g$ for nitrogen physisorption, respectively. Because of the higher polarity of water in comparison to the chloroform solution, the larger crystallite sizes of aqueous solutions in CMK-3 compared to the organic solution can be explained by the nucleation occurring outside of the pores (**1**−**12**). In comparison, the crystallite sizes of aqueous solution-derived MPt

(53) Dahmani, C. E.; Cadeville, M. C.; Sanchez, J. M.; Moran-Lopez, J. L. *Phys. Rev. Lett.* **1985**, *55*, 1208.
(54) Sanchez, J. M.; Moran-Lopez, J. L.; Leroux, C.; Cadeville, M. C. *J. Phys. C* **1988**, *21*, L1091.
(55) Massalski, T. B. *Binary Alloy Phase Diagrams*, 2nd ed.; ASM International: Materials Park, OH, 1990; p 1752.

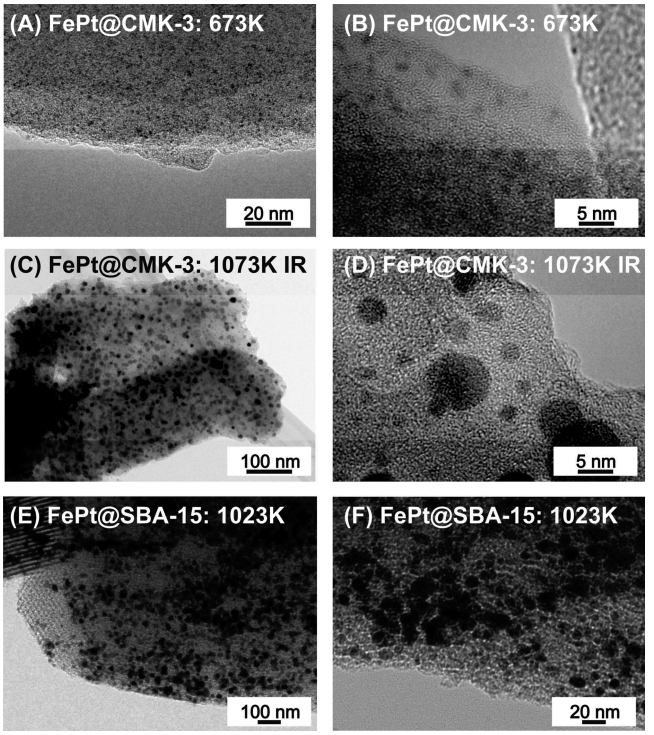


**Figure 2.** Transmission electron micrographs of FePt@CMK-3 composites prepared by chloroform solution and heat treated at 673 K (**13**: A, B) and 1073 K IR (**14**: C, D) and FePt@SBA-15 composites (**27**: E, F) annealed at 1023 K in a hydrogen atmosphere.

particles in mesoporous silica show better agreement to the pore diameter of 9.4 nm as estimated by nitrogen physisorption measurements (**25**−**36**).

The X-ray powder diffraction results were confirmed by TEM measurements for FePt nanocomposites (Figure 2 and the Supporting Information 8). One can observe that the intermetallic nanoparticles are well dispersed inside the mesoporous matrix. However, for FePt@CMK-3 ($CHCl_3$) composites (**14**) annealed at 1073 K in IR furnace (Figure 2C, D) a bimodal size distribution of 2−3 and 8 nm, respectively was detected. In relation to the monodisperse size distribution in the range of 2 nm for fcc particles (**13**) annealed at 673 K (Figure 2A, B) an interaction to the porous carbon matrix during the fct phase formation can be assumed, which will be discussed in the next section. In contrast, fct FePt nanoparticles annealed for 1 h at 1023 K (**27**) show a narrow size distribution (Figure 2E, F).

In addition, the weak chloroform-solvent to silica-matrix interactions cause a high rate of nucleation (**37**−**48**), leading to small crystallite sizes ( < 2 nm). Thus, further discussions will be focused on the preparation of MPt composite structures in CMK-3 using chloroform solutions (**13**−**24**) and for aqueous solution derived intermetallic systems in SBA-15 (**25**−**36**).

The fct phase formation and resulting crystallite size is also dependent on the specific MPt intermetallic system and the thermal treatment regime used to process and anneal that system.

In general, the crystallite sizes for the FePt and CoPt systems increase during the annealing at 873 K-1073 K by the indirect treatment (**1**−**8**, **25**−**32**). The fct modification is entirely present for FePt systems after thermal treatment at 1023 K in the regular (**15**, **27**) and at 1073 K in the IR furnace (**14** $\mathbf{H_2}$, **26**) for FePt@CMK-3 ($CHCl_3$) and FePt@SBA-15 ($H_2O$) composites (Figure 1). These results show good agreement to previous studies for the synthesis of FePt in ordered mesoporous silica.[25] CoPt nanoparticles in CMK-3 ($CHCl_3$) treated at 1023 K (**31**) also form the fct phase; however, CoPt containing silica compounds form a platinum-rich $CoPt_3$ phase after the same treatment. The latter indicates a phase separation process of cobalt and platinum during the first heating ramp to 673 K forming crystalline fcc $CoPt_3$ and a X-ray amorphous Co phase (**29**). A similar phase separation was found for NiPt (**33**−**36**). The fcc Ni phase was detected beside the platinum rich NiPt phase for all composite structures during the reductive annealing process. The NiPt nanoparticles synthesized inside CMK-3 ($CHCl_3$) remain amorphous after crystallization at 873 K (**22**−**24**). In comparison, silica templated NiPt was crystalline with grain sizes in the range of 8.2−10.4 nm, dependent on the specific thermal treatment conditions (**33**−**36**).

In the present study, for comparison with the conventional furnace, an infrared furnace was used for faster heating times to minimize particle aggregation. Experiments reported in Table 2 (1073 IR) show FePt composites with smaller crystallite sizes of 7.8 nm (**14** $\mathbf{H_2}$, CMK-3) and 8.3 nm (**26**, SBA-15) as compared to 9.6 nm (**15**) and 10.6 nm (**27**) for those annealed in a conventional furnace. However, the phase transformation for the IR heat treated FePt@SBA-15 (**26**) composite is incomplete, due to the weak (001) and (110) peak intensities as well as the less drastic (111) peak shift when compared to fct-FePt compounds synthesized in a regular furnace (**27**). In comparison, the CoPt particles in CMK-3 ($CHCl_3$) form the fct phase and show a slight decrease in size for the IR treatment (**18**). The $CoPt_3$ phase found in silica has an increased size after IR annealing (**30**). To investigate the influence of gas phase composition during thermal treatment, we also heat-treated FePt@CMK-3 composites in an inert atmosphere up to 1073 K in an IR furnace (**14 Ar**, Figure 1B−Ar). The crystallite sizes of the resulting FePt nanoparticles are significantly smaller (**14 Ar**: 2 nm) than hydrogen annealed systems (**14** $\mathbf{H_2}$: 7.8 nm).

For a comprehensive study, the MPt structures were also heat-treated in a single-step procedure up to 1073 K in an IR furnace for the carbon matrix (**16**) and up to 1023 K in a regular furnace for the SBA-15 system (**28**, Scheme 1, direct treatment). The different synthesis conditions were selected due to the incomplete phase transformation of FePt in SBA-15 using the IR technique and the particle aggregation found in the connected pore structure of CMK-3 after the longer-duration regular treatment, as discussed previously. The resulting FePt crystallite sizes of 7.3 nm for CMK-3 (**16**) and 7.5 nm for SBA-15 (**28**) composites are smaller than particles synthesized by indirect treatment, and transformation into fct phase is complete. Similarly, the grain size of CoPt@CMK-3 (**20**) composites synthesized by direct

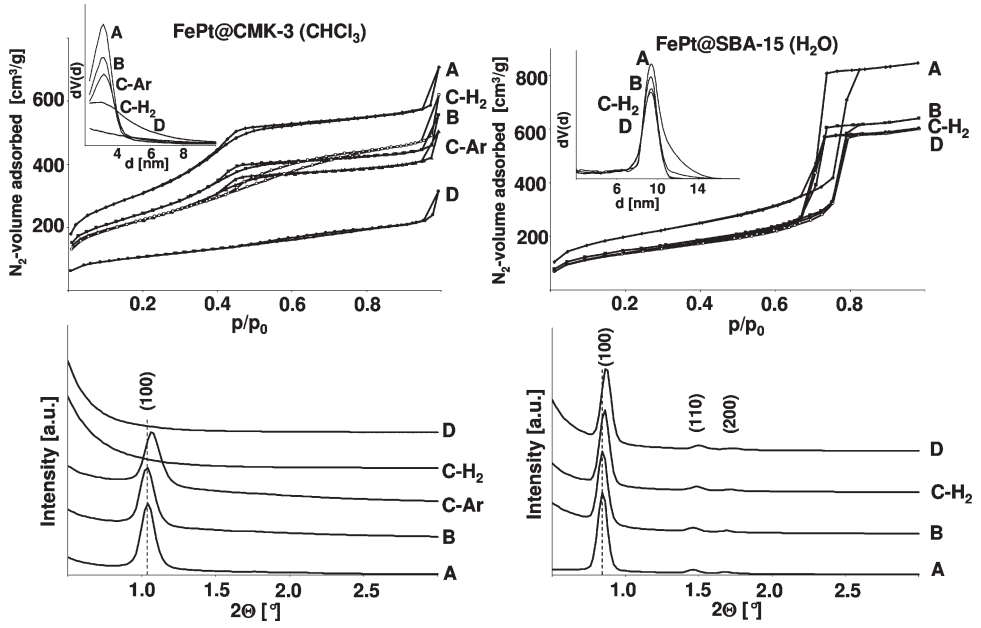


**Figure 3.** $N_2$-physisorption and small-angle X-ray diffraction of pristine mesoporous carbon (left, A) and silica (right, A) and (B) FePt@CMK-3 (**13**−**15**: left) and SBA-15 composites (**25**−**27**: right) annealed at 673 K, (C−Ar) 1073 K under argon, and (C−$H_2$) hydrogen atmosphere using IR furnace and (D) at 1023 K.

**Table 3. Adsorption Properties and Lattice Constants of Mesoporous Host for Pristine and FePt Composites in Dependence on the Thermal Treatment Conditions**

| | | FePt@CMK-3 | | | | | | FePt@SBA-15 | | | |
|---|---|---|---|---|---|---|---|---|---|---|---|
| | | indirect | | | | direct | | indirect | | | direct |
| | CMK-3 | 673 | 1073 IR-Ar | 1073 IR-$H_2$ | 1023 | 1073 IR | SBA-15 | 673 | 1073 IR | 1023 | 1023 |
| $S_g$ ($m^2$/g) | 1102 | 872 | 797 | 810 | 381 | 684 | 722 | 536 | 495 | 508 | 519 |
| $d_{pore}$[a] (nm) | 3.2 | 3.2 | 3.2 | broad | broad | broad | 9.4 | 9.4 | 9.4 | 9.4 | 9.4 |
| $V$ ($cm^3$/g) | 0.89 | 0.69 | 0.64 | 0.74 | 0.34 | 0.74 | 1.3 | 0.99 | 0.92 | 0.92 | 0.91 |
| $a$ (nm)[b] | 9.8 | 9.8 | 9.6 | | | | 12.1 | 12.1 | 11.9 | 11.9 | 11.9 |

[a] Pore diameter estimated by adsorption branch for CMK-3 and SBA-15 structures. [b] Lattice constant calculated from (100) peak for hexagonal systems in small-angle X-ray diffraction.

treatment is significantly smaller (5.4 nm) than those made in the indirect manner; however, the fct phase transformation is incomplete. In contrast, fct ordered CoPt nanoparticles about 10.2 nm in diameter were obtained in silica after direct treatment at 1023 K (**32**).

The mass ratio of FePt nanoparticles inside the mesoporous template was estimated by EDX measurements. The FePt content for silica composites remains almost constant during reductive treatment at 26 wt % (**25**−**28**). In contrast, the FePt content strongly increases from 23 wt % (**13**) up to 57 wt % (**15**) with increasing reduction temperature. These results are confirmed by nitrogen physisorption measurements that will be discussed in the following.

**Structure of the Mesoporous Matrix: Small-Angle X-ray Powder Diffraction (SAXD)/$N_2$-Physisorption.** Ordering and porosity of pristine and FePt loaded mesoporous silica (**25**−**28**) and CMK-3 structures (**13**−**16**) were investigated by SAXD and $N_2$-physisorption measurements presented in Figure 3 and Table 3 (MPt: Supporting Information 9−11). FePt containing SBA-15 and CMK-3 composites prepared by the indirect treatment at 673 K (**13, 25**) show ordered pore structures with lattice constants of 12.2 and 9.8 nm and pore sizes in the range of 9.4 and 3.2 nm corresponding to the pristine materials. Specific surface area and pore volume of silica and carbon composites decrease down to 76 and 80% related to the mass fraction of intermetallic nanoparticles. However, no ordering for FePt@CMK-3 structures annealed at 1023−1073 K under reductive conditions (**14 $H_2$, 15**) can be observed because of the absence of the (100) peak in small-angle XRD and the broad pore size distributions estimated by $N_2$-physisorption measurements. The latter is related to the catalytic reductive removal reaction of carbon matrix in the presence of FePt nanoparticles. However, a short duration in IR furnace at 1073 K (**14 $H_2$**) causes a significantly lower decrease in specific surface area and pore volume compared to regular treatment at 1023 K (**15**). In contrast, ordering and pore structure remain intact by treating the composite structure in inert atmosphere up to 1073 K (**14 Ar**). According to XRD measurements, the resulting nanoparticles show significantly smaller FePt crystallite sizes in the range of 2−3 nm. In comparison, ordering and pore system for FePt@$SiO_2$ composites stay intact during reductive treatment up to 1073 K (**26**−**28**). Nevertheless,

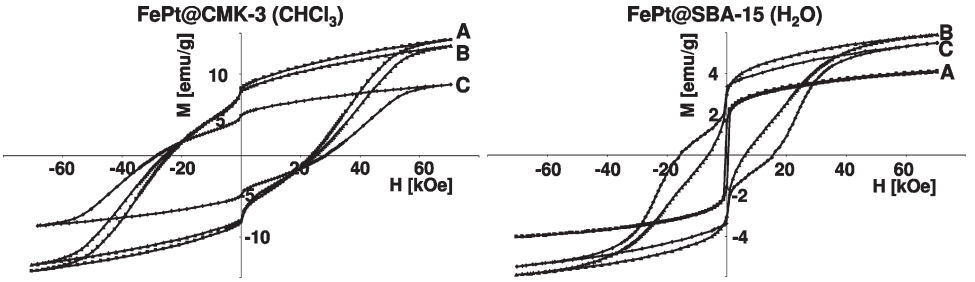


**Figure 4.** Room-temperature magnetization demagnetization curves of FePt@CMK-3 (**14**−**16**: left) and FePt@SBA-15 composites (**26**−**28**: right) annealed at (A) 1073 K IR and (B) 1023 K by indirect treatment and (C) at 1073 K IR for carbon and 1023 K for silica composites prepared by direct treatment, respectively.

**Table 4. Room-Temperature Coercivities [kOe] for MPt Carbon and Silica Composites Annealed at 673−1073 K**

| | FePt | | | | | CoPt | | | | NiPt | | | |
|---|---|---|---|---|---|---|---|---|---|---|---|---|---|
| | indirect | | | | direct | indirect | | | direct | indirect | | | direct |
| | 673 | 1073 IR Ar | 1073 IR $H_2$ | 1023 | 1073 IR /1023 | 673 | 1073 IR | 1023 | 1073 IR /1023 | 673 | 873 IR | 873 | 873 IR /873 |
| CMK-3[a] | 0.08 | 0.62 | 23.94 | 25.53 | 28.35 | 0.07 | 0.70 | 1.26 | 1.39 | 0.02 | 0.01 | 0 | 0.03 |
| SBA-15[b] | 0.11 | | 0.51 | 6.23 | 15.60 | 0.28 | 0.33 | 0.30 | 2.07 | 0.08 | 0.27 | 0.28 | 0.16 |

[a] Composites prepared by infiltration of chloroform. [b] Composites prepared by infiltration of aqueous precursor solutions into ordered mesoporous host.

lattice constants decrease down to 11.9 nm due to sintering effects in porous silica matrix at these temperatures.[56]

**Magnetic Investigations of MPt Composites.** Isothermal hysteresis loops of platinum containing intermetallic CMK-3 ($CHCl_3$) and SBA-15 ($H_2O$) composites at room temperature are presented in Figure 4 and the Supporting Information 12−18, and corresponding coercivities are summarized in Table 4. The resulting magnetic properties are strongly dependent on the intermetallic system, the mesoporous matrix, and the thermal treatment conditions, which will be discussed in the following. The coercivities of FePt@CMK-3 composites are determined by the degree of crystallinity and phase structure. Carbon and silica composites prepared at 673 K show relatively small coercivities of 0.08 kOe (**13**) and 0.11 kOe (**25**), respectively, corresponding to their almost X-ray amorphous or soft magnetic fcc FePt structure. In comparison, FePt@CMK-3 materials annealed at 1023 K-1073 K show extremely high coercivities up to 25.53 kOe (**15**) and 28.35 kOe (**16**) for indirect and direct treatment, respectively, because of the highly ordered intermetallic fct structure as detected by X-ray powder diffraction. The drop in magnetization at zero field can be related to the size distribution of hydrogen treated FePt particles in the carbon matrix, as seen by TEM, or an incomplete phase transformation into fct phase and particle motion inside the magnetic field, causing different remanence and coercivity values.[57] For comparison, the FePt@CMK-3 composite was annealed in an inert atmosphere of Ar at 1073 K in IR furnace. Those particles show a considerably smaller coercivity of 0.62 kOe (**14 Ar**) as compared to the 23.94 kOe (**14 $H_2$**) found in hydrogen treated compounds. The latter can be related to the smaller crystallite sizes of argon annealed structures as demonstrated by X-ray and TEM measurements. Nevertheless, a coercivity of 0.62 kOe for argon post-treated composites (**14 Ar**) is larger than those annealed at 673 K in $H_2$ (**13**: 0.08 kOe), indicating at least partial transformation into the fct phase. This can be understood as the coercivity is proportional to a materials anisotropy constant, and the fct phase has a higher anisotropy constant than the fcc phase.[58]

In general, FePt nanoparticles synthesized inside mesoporous silica (**26**−**28**) show smaller coercivities and saturation magnetization than comparable carbon templated materials (**14**−**16**), with the most pronounced difference in samples prepared via the indirect route. However, particles synthesized in a silica host by direct treatment at 1023 K offer a significantly higher coercivity of 15.6 kOe (**28**) than metallic structures indirectly treated at 1023 K (**27**: 6.23 kOe) and 1073 K in IR (**26**: 0.51 kOe). In comparison, previously reported preparation methods of FePt nanoparticles inside SBA-15 by multiple infiltrations of DMSO solution have coercivities of 0.28 kOe.[25]

The magnetic properties of CoPt composites differ significantly from FePt, although both intermetallic materials have similar anisotropic constants.[10] For example, room temperature coercivities for CoPt particles incorporated into carbon matrices are as low as 0.7 kOe (**18**) for indirect and 1.39 kOe (**20**) for direct treatment at 1073 K in an IR furnace as compared to 23.94 kOe (**14**) and 28.35 kOe (**16**) for similarly prepared FePt structures. Additionally, the drop in magnetization at zero field is more pronounced in CoPt systems and nearly all samples exhibit some shift of the hysteresis loop along the field axis. The shoulder in M-H is indicative of the particle size distribution demonstrated by TEM measurements

(56) Krawiec, P.; Kaskel, S. *J. Solid State Chem.* **2006**, *179*, 2281.
(57) Tauxe, L.; Mullender, T. A. T.; Pick, T. *J. Geophys. Res.* **1996**, *101*, 571.
(58) Skomski, R. *J. Phys.* **2003**, *15*, R841.

(see Supporting Information 7) and the exchange bias effect could result from the possible existence of a second (antiferro)magnetic species.[57,59] The room-temperature coercivity of 0.33 kOe (**30**) for CoPt@SBA-15 structures prepared by indirect treatment indicates only weak ferromagnetism and appears to be independent of the thermal treatment type. These results are related to the formation of a soft magnetic $CoPt_3$ phase as estimated by X-ray powder diffraction. In contrast, the direct-method treated composites annealed at 1023 K have coercivities up to 2.07 kOe (**32**) because of the hard magnetic fct-CoPt phase. However, a drop in the hysteresis loop at zero field and exchange bias phenomena similar to CoPt@CMK-3 composites was observed, probably for the same reasons as discussed above.

NiPt shows very weak ferromagnetism with coercivity values of only 0.03 kOe (**24**) for CMK-3 and 0.26 kOe (**34**) for SBA-15 composites. The latter is caused by the formation of soft magnetic Pt-rich NiPt phase for silica and the almost X-ray amorphous NiPt structure inside mesoporous carbon. However, a direct comparison to magnetic properties of FePt and CoPt is rather complicated, because of the lower annealing temperature for NiPt structures.

**Catalytic Gas-Phase Hydrogenation.** Gupta and coworkers reported that FePt supported on silica catalyzes the hydrogenation of 1-decene.[39] Hence, activity, selectivity and stability of two different materials comprising the same FePt loading and support, i.e., Fe/Pt@SBA-15 with intermetallic fct phase (**50**) and with disordered fcc phase (**49**), were tested in catalytic hydrogenation of acetylene in the presence of ethylene.

Both tested catalysts are active for gas-phase hydrogenation, the fcc material (**49**) being more active in the first and second temperature cycle as evident from higher conversion of acetylene (Figure 5) and hydrogen (see Supporting Information 19). Although the less active catalyst with fct phase (**50**) remains stable in activity for about 150 h as apparent from conversion shown vs time-on-stream (Figure 5, Supporting Information 19), the higher activity of the fcc phase (**49**) fades after the first two temperature cycles and converges to a similar activity as for the fct material (**50**). One possible explanation is that under reaction conditions at slightly elevated temperature an annealing process occurs that leads to a decrease in performance of the disordered fcc phase (**49**). In contrast, the ordered intermetallic fct (**50**) remains stable under reaction conditions attributed to the ordered phase produced by reduction at 1023 K for 1 h.

The two materials differed in selectivity throughout the experiment as shown for the initial temperature cycle (Figure 6) and the third cycle measured under the same conditions (see Supporting Information 20) and indicated

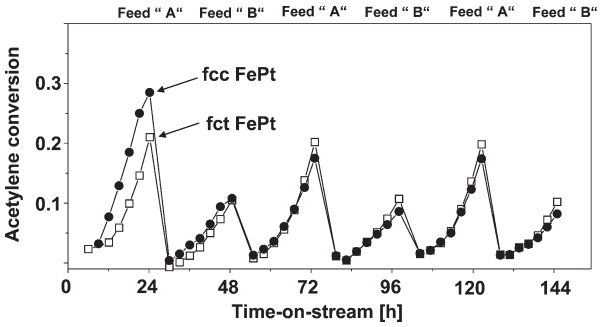


**Figure 5.** Acetylene conversion vs time-on-stream in hydrogenation of a mixture of acetylene/ethylene using two different FePt@SBA-15 materials (fcc-FePt (**49**); fct-FePt (**50**)) in a continuous fixed-bed reactor operated in repeated temperature cycles between 313 and 373 K feeding a gas mixture with a hydrogen content of 3.4% (condition A) or 2.1% (condition B).

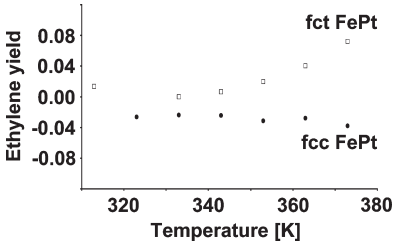


**Figure 6.** Ethylene yield vs temperature recorded in the 1st temperature cycle of hydrogenation of a mixture of acetylene/ethylene using two different FePt@SBA-15 materials (fcc-FePt (**49**); fct-FePt (**50**)) in a continuous fixed-bed reactor operated in repeated temperature cycles; a gas mixture containing 3.4% $H_2$, 1.7% acetylene, and 42.9% ethylene was dosed (condition A); negative yield indicates the net consumption of ethylene.

by the different ethylene yields. The curves represent the ratio between formed ethylene and consumed acetylene. Hence, positive values relate to net formation of ethylene, i.e., selective conversion of acetylene to ethylene, whereas negative values result from net ethylene consumption, i.e., the conversion of both acetylene and ethylene into ethane. As indicated by the graphs (Figure 6 and Supporting Information 20), the ordered intermetallic fct-FePt phase (**50**) selectively hydrogenates acetylene into ethylene also in the presence of excess ethylene with increasing the temperature, whereas the fcc-FePt catalyst (**49**) favors total hydrogenation to ethane. This pronounced difference of more selective hydrogenation over the fct phase (**50**) catalyst is preserved also after extended time-on-stream ($t = 50$ h, see Supporting Information 20) when the activity of the fcc phase (**49**) has decreased already remarkably.

The presented catalytic data suggest that the intermetallic fct-FePt phase (**50**) performs superior to the disordered fcc phase (**49**) both with respect to stability and selectivity. Nevertheless, it must be also mentioned that both tested materials were less active and less selective than Pd/ZnO catalysts tested under the same reaction conditions.

## Conclusions

Summarizing, we have presented a new synthesis strategy for the preparation of magnetic MPt nanoparticles

(59) Salabas, E. L.; Rumplecker, A.; Kleitz, F.; Radu, F.; Schueth, F. *Nano Lett*. **2006**, *6*, 2977.
(60) Choi, M.; Heo, W.; Kleitz, F.; Ryoo, R. *Chem. Commun*. **2003**, 1340.
(61) Jun, S.; Joo, S. H.; Ryoo, R.; Kruk, M.; Jaroniec, M.; Liu, Z.; Ohsuna, T.; Terasaki, O. *J. Am. Chem. Soc*. **2000**, *122*, 10712.
(62) Cukic, T.; Kraehnert, R.; Holena, M.; Herein, D.; Linke, D.; Dingerdissen, U. *Appl. Catal*. **2007**, *323*, 25.

inside the pores of ordered mesoporous silica and carbon materials. The influence of the mesoporous matrix related to the solvent polarity as well as the thermal treatment conditions to the phase transformation process and crystallite sizes of resulting MPt nanoparticles were investigated. It was demonstrated that aqueous precursor solution is appropriate for the synthesis of silica composites whereas organic chloroform solutions are suitable for the preparation of more hydrophobic carbon composites. Room-temperature coercivities of heat treated fct FePt nanoaprticles inside porous carbon templates offer extraordinary high room-temperature coercivities up to 28.35 kOe, which is among the highest ever reported values. The pore structure of CMK-3 changes significantly during phase transformation process in hydrogen atmosphere indicating a catalytic hydrogenation of the carbon structure. In comparison, silica templated fct FePt nanoparticles show lower coercivities. However, SBA-15 matrices remain intact during reductive treatment forming ordered alloys. A significantly higher selectivity of ordered fct FePt compared to disordered fcc alloy in gas phase acetylene to ethylene hydrogenation could be verified for the first time. Thus, templated ferromagnetic MPt systems are promising advanced selective catalysts because of the high porosity of the versatile mesoporous matrix and the precise control of phase composition and particle size of bifunctional ferromagnetic MPt catalysts.

**Acknowledgment.** Financial support by the German Academic Exchange Service (DAAD) is gratefully acknowledged. Research at the Nebraska Center for Materials and Nanoscience-NCMN were supported by the National Science Foundation MRSEC (DMR-0820521) (T.A.G.) and Department of Energy (DE-FG02-04ER46152) (R.S. and D.J.S.).

**Supporting Information Available:** An additional table and 19 figures that contain the following material: (S1) X-ray powder diffraction patterns of CoPt/NiPt@CMK-3 ($CHCl_3$) composites (S2, S3) XRD patterns of MPt @CMK-3 ($H_2O$) composites (S4) XRD patterns of CoPt/NiPt@SBA-15 ($H_2O$) composites (S5) XRD patterns of FePt/CoPt@SBA-15 ($CHCl_3$) composites (S6) Water vapor physisorption measurements of pristine SBA-15 and CMK-3 composites (S7) Transmission electron micrographs of CoPt@CMK-3 ($CHCl_3$) composites (S8) Transmission electron micrographs of FePt@CMK-3 ($H_2O$) composites (S9) Small angle X-ray diffraction patterns of CoPt/NiPt@CMK-3 ($CHCl_3$) composites (S10) Small angle X-ray diffraction MPt@CMK-3 ($H_2O$) composites (S11) Small angle X-ray diffraction patterns of MPt@SBA-15 composites (S12; 13) Isothermal magnetization-demagnetization curves of FePt@CMK-3 ($CHCl_3$) composites (S14) Room temperature magnetization-demagnetization curves of CoPt@CMK-3 and CoPt@SBA-15 composites (S15) Room temperature magnetization-demagnetization curves of NiPt@CMK-3 ($CHCl_3$) and NiPt@SBA-15 ($H_2O$) composites (S16) Room temperature magnetization-demagnetization curves of MPt@CMK-3 ($CHCl_3$) and MPt@SBA-15 ($H_2O$) composites (S17) Room temperature magnetization-demagnetization curves of CoPt/NiPt@SBA-15 ($CHCl_3$) composites (S18) Room temperature coercivities of CoPt/NiPt@SBA-15 ($CHCl_3$) composites (19) Hydrogen conversion vs TOF in hydrogenation of a mixture of acetylene/ethylene of FePt@SBA-15 composites (S20) Ethylene yield vs temperature recorded in the 3rd temperature cycle of hydrogenation of a mixture of acetylene/ethylene using FePt@SBA-15 composites (PDF). This material is available free of charge via the Internet at http://pubs.acs.org.